

Focusing of Surface Plasmon Wave for Small-Molecule Sensing

Hongrui Shan, Hailang Dai,* Qiheng Wei, and Xianfeng Chen*

Miniaturized manipulation and control of surface plasmon waves have long been a desirable goal. However, conventional nanomethods have high losses and uncontrollable outcomes, which limit their utility in light–matter interaction. To overcome these challenges, a method for achieving directional propagation and concentration of surface plasmon waves using nanostructures is proposed. By focusing the transmission of surface plasmon waves on the tip of a nanotriangle, the power of light is enhanced by an order of magnitude. This design can be applied to sensing small molecules, both living and nonliving. It is believed that this approach can be used to realize real-time, integrated biosensing on miniaturized chips.

1. Introduction

Since the 2000s, with the development of nanotechnology, various nanomaterials with a feature size in the range of 1–300 nm have been used in a wide range of areas.^[1,2] Significant efforts have been devoted to studying the strong light–matter interactions at the nanoscale.^[3] Noble metal nanomaterials such as gold, silver, and copper have attracted considerable interest because of their special properties like catalytic activity, fluorescence characteristics, and surface plasmon (SP).^[4–6] Therein, the SPs are extremely sensitive to properties of the nanoparticles and the surrounding medium, resulting in their good performance as sensors.^[7–9] For extended metal surfaces, this gives rise to surface plasmon polaritons (SPPs), a state of evanescent wave, which are localized on the surface of metal by the interaction of electrons and photons, and surface plasmon waves (SPWs) propagating at the metal–dielectric interface. For metal nanoparticles, the response arises from localized surface plasmons (LSPs), whose resonances depend on the particle material, size, and shape. When a metal nanoparticle surrounded by a dielectric is excited by electromagnetic radiation, its free electrons will oscillate

collectively through resonant interaction with the incident electromagnetic field. This process is called localized surface plasmon resonance (LSPR)^[6,10–12] and shows broad potential for application in nanophotonic,^[13] materials science,^[14] life science,^[15] and environmental engineering.^[16] Based on the control of SPWs of nanoparticles, many practical applications have been reported, such as surface-enhanced Raman scattering (SERM),^[13–16] display technology,^[17] medical diagnosis and therapy,^[2,18–21] biosensing and bioimaging,^[7–9,22] solar cells,^[23] micro-/nanodevices,^[24–26] and so on.

Moreover, one of the most important properties of SP is its capability to overcome the classical diffraction limit and manipulate light at the subwavelength scale. A feature of SPs is that they are localized at much smaller scales than the wavelength of incident light, which is of significant interest to the developments in highly-integrated photonics,^[27–29] and in data storage applications.^[30,31] Thus, localizing or confining light in a smaller area is critical to numerous fields, including integrated photonics, subwavelength optics,^[32] optical data storage, and super-resolution microscopy techniques such as tip-based near-field scanning microscopy (SNOM)^[33,34] and lithography.^[35–37] However, the large losses due to the oscillatory absorption of free electrons and small transmission distance make it difficult to achieve a strong local field enhancement and perfect transmission feature without high transmission loss, which limits further application. Moreover, the cumbersome and sophisticated mechanical systems required for manipulating the tip of tip-based SNOM to probe the sample of interest severely restricts the potential for miniaturization.^[38,39] Additionally, the sample must be pretreated and fixed for analysis with tip-based SNOM, causing difficulties with implementing real-time detection of changes in the sample.

In this work, we have developed gold nanostructures with nanodisk, cuboidal, and triangular geometries that enable the focusing and guiding of SPWs. Moreover, the sample of interest can be transported to the focusing region by the microchannel without the cumbersome mechanical manipulation system, permitting real-time analysis. Through numerical simulations and experiments with transverse magnetic (TM)/transverse electric (TE) polarization (S2–S4, Supporting Information), we have demonstrated that SPWs can be transported between different nanostructures with the bulk of SPW power being focused at the tip of the nanostructure. Notably, we have achieved perfect transmission features without loss due to eigenmode resonance and have observed an order of magnitude enhancement in the

H. Shan, H. Dai, Q. Wei, X. Chen
State Key Laboratory of Advanced Optical Communication Systems and Networks
School of Physics and Astronomy
Shanghai Jiao Tong University
Shanghai 200240, China
E-mail: hailangdai@sjtu.edu.cn; xfchen@sjtu.edu.cn

© 2023 The Authors. Advanced Photonics Research published by Wiley-VCH GmbH. This is an open access article under the terms of the Creative Commons Attribution License, which permits use, distribution and reproduction in any medium, provided the original work is properly cited.

DOI: 10.1002/adpr.202300165

power of the electromagnetic field at the focusing tip, as shown in S5, Supporting Information. The transfer distance and orientation of the focusing point can be tailored for specific applications. Furthermore, we have designed and implemented double nanostructures for enhanced light–matter interaction, which has been applied to the development of a sensor capable of detecting and distinguishing nonliving and living components.

2. Results and Discussions

2.1. The Principle of Nanostructures

According to the Maxwell equations for a nanodisk, we consider a simplified model where the thickness of the disk is much larger than its radius and the dielectric constant remains unchanged with \vec{e}_θ direction. Therefore, the amplitude of the field only changes with r direction.

$$\begin{cases} \vec{E}_{(r,\theta,z,t)} = \vec{E}_{(r)} e^{i(\beta z - \omega t)} \\ \vec{H}_{(r,\theta,z,t)} = \vec{H}_{(r)} e^{i(\beta z - \omega t)} \end{cases} \quad (1)$$

where $\beta = k_0 \sqrt{\epsilon} \sin(\gamma)$ is the z component of the wave vector k , and γ represents the angle of incidence.

For a nonmagnetic system without free charge and current, we can get the Helmholtz equation of E_r and E_θ , respectively.

$$\begin{cases} \frac{\partial^2 E_r}{\partial r^2} + (k_0^2 \epsilon_r - \beta^2) E_r = 0 \\ \frac{\partial^2 E_\theta}{\partial r^2} + (k_0^2 \epsilon_r - \beta^2) E_\theta = 0 \end{cases} \quad (2)$$

where $k_0 = \omega \sqrt{\mu_0 \epsilon_0}$ is the propagation constant in vacuum. For a system of two nanodisks, the coupling coefficient M can be expressed as

$$M = \langle \varphi_1 | \varphi_2 \rangle \quad (3)$$

where φ_1 and φ_2 are the normalized electric field functions of the two nanodisks. The coupling coefficient M with different radii and different distances is shown in Figure S7, Supporting Information. We found that two nanodisks with 50 nm distance and 100 nm radius can achieve excellent SPW transport. Based on this fundamental analysis, we designed the numerical simulation using finite difference time domain (FDTD) software. The surface of the structure was detected by a monitor. The boundary conditions were implemented using the perfectly matched layer (PML) approach. In the results, the power of electromagnetic field has been enhanced 109.6 and 21.4 at the focusing point of structure bottom using the nanodisks–nanotriangle and nanodisks–nanocuboid–nanotriangle under light illumination, respectively, as shown in Figure 1a,f. A detailed description of numerical simulation is presented in S1–S5, Supporting Information.

2.2. Fabricated Nanostructures and Numerical Simulations

In our research, we selected focused ion beam (FIB) over electron beam lithography (EBL) because of its ability to perform 3D fabrication, direct-write capabilities, low cost, and wider material compatibility, which were crucial for achieving the desired nanoscale structures. We also added related descriptions in the article. Nanodisks with a diameter of 500 nm were designed and

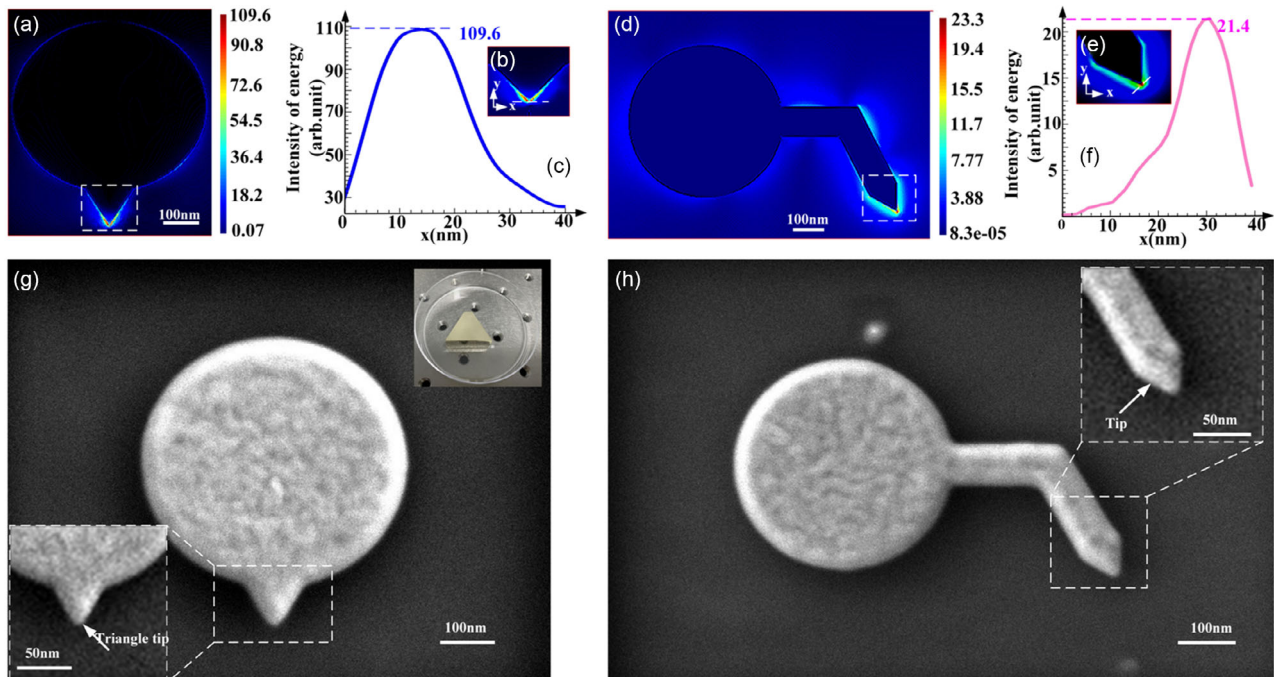


Figure 1. a,d) Simulations of a 500 nm-sized gold nanodisk with a 50 nm gold triangle tip and a 50 nm zigzag with a gold triangle-tipped rod, respectively. b,e) Magnified figures of the area in the dotted box of (a,d), respectively. c,f) The energy intensity distributions on the transversal dotted line of (b,e), respectively. g,h) The SEM image of the manufactured nanostructures, respectively. Scale bar, 100 nm.

processed on substrates of the SiO₂ prism using FIB. Under the 860 nm wavelength of TM polarization laser illumination in numerical simulation by FDTD software, Figure 1a,d shows the energies distribution of light field on the bottom layer of 500 nm-sized gold nanodisks with a 50 nm gold triangle tip and a 50 nm zigzag with a gold triangle tipped rod, respectively. The incident light was focused into the tips with the help of a prism under the nanostructures. The corresponding light field distributions on the transversal dotted lines are shown in Figure 1c,f. The nanostructure is able to guide the incident light so that it converges at the tip (Figure 1d). The sample fabrication was effectively accomplished using FIB machining, as shown in Figure 1g,h. To evaluate the convergence effect, a prism with a gold nanodisk with a diameter of 500 nm was carved onto it.

2.3. Optics Testing and Applications

2.3.1. Optics Testing

The scanning near-field optical microscope (SNOM, Ntegra Solaris of NT-MDT) with 350–950 nm wavelength band of laser source (GLOphotonics Comblas-VIS) was used to detect the characteristics of the sample through FIB process. **Figure 2a** illustrates the energy field diagram of the nanodisk experiment with a sharp tip, which showcases a phenomenon of light field focusing under irradiation with a 1 mW 350–950 nm wavelength band laser source. **Figure 2b** shows the energy field distribution on the white dotted transversal in **Figure 2a**. The relative light intensity of the tip of nanodisk–nanotriangle with stronger light is 10.5, which is 4.2 times that at the edge of the nanodisk with an

intensity of 2.5. The calculation results in **Figure 2c** reveal that the corresponding tip light strength is 109.6 and the edge strength is 13.8, indicating a 7.9-fold enhancement. **Figure 2d**, e,f presents the comparable experimental findings for the gold nanodisk with nanocuboid–nanotriangle under the same experimental condition. As depicted in **Figure 2f**, the corresponding simulation data displays 11.3-fold enhancement with intensity of 21.4 on point E₂ and 1.9 on point C₂. By combining the numerical simulation and experimental results, we can achieve two nanostructures to realize SPW directional propagation and concentration, which enable the energy of light focusing and enhancement. Additionally, the property of the prepared two nanostructures can be used to strongly enhance the light-matter interaction. Therefore, the directional propagation and concentration of nanostructures could be effectively adapted for biosensing, such as the detection and monitoring of molecule and biomolecule interactions by enhancing the light–matter interaction.

2.3.2. Applications

According to the above, the light–matter interaction will be enhanced via our nanostructure to detect or monitor the molecular interaction. In order to demonstrate the benefit of this technology in detection and monitoring, the common fluorescent dye rhodamine 6G (R6G) and a common biological molecule protoporphyrin IX (PpIX) was used to measure enhancement in fluorescence intensity and monitor the molecular interaction based on light–matter interaction by SNOM with a 350–950 nm wavelength band laser source (GLOphotonics Comblas-VIS),

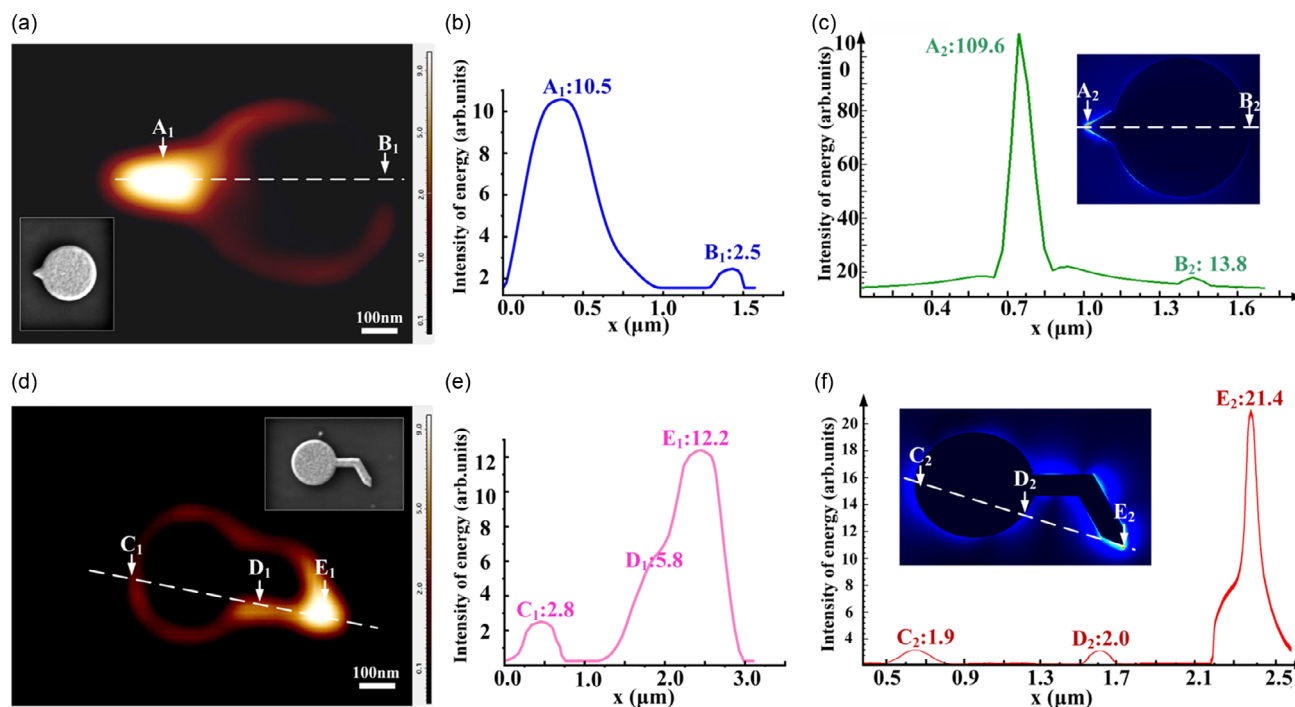


Figure 2. Strong near-field enhancement in the sharp corner of the gold optical nanostructures. a,d) SNOM images of the manufactured nanodisks with nanotriangle and nanocuboid–nanotriangle, respectively. b,e) Experimental energy intensity distributions on the transversal dotted line of graph (a,d), respectively. c,f) The calculations of energy intensity distributions on the transversal dotted line of the simulation insets, respectively. Scale bar, 100 nm.

respectively. First, in our experiment, a 10 mL dose of R6G at 4.3×10^{-17} g mL⁻¹ was injected and transported into the nanostructure by prepared microchannel, as depicted in **Figure 3a**. A detailed protocol for preparation of the highly dilute R6G solution is provided in S8, Supporting Information, and the observation of single-step photobleaching is shown in S10, Supporting Information. We then measured the intensity of fluorescence from points A and B on the structure when the 350–950 nm wavelength band laser beam illuminated the nanodisks–nanotriangle structure. As shown in **Figure 3a**, point A is the tip of the nanotriangle and point B is a point on the nanodisk. According to the detection results, the fluorescence intensity of R6G has been enhanced due to the enhancement of light–matter interaction at the tip of structure compared with point B, as shown in **Figure 3b,c**. Finally, the corresponding light energy field of the nanodisk with R6G is shown in **Figure 3b** obtained with SNOM. Fluorescence at point A is stronger with a relative light intensity of 4.90, which is 2.59 times that at the edge of the nanodisk (point B) with an intensity of 1.89. Simultaneously, we examined the fluorescence spectral signals of R6G on the sharp corner and nanodisk edges separately, as shown in **Figure 3c**. The energy measured at point A is 2.85 times higher than point B of the nanodisk. The fluorescence intensity recorded at points A and B

remains stable throughout ten repetitions of the experiment, as shown in **Figure 3d**, suggesting that single-molecule interactions can be reliably monitored by our structure.

PpIX is ubiquitously present in all living cells in small amounts as a precursor of heme.^[40] PpIX has some biological functions of its own, and PpIX-based strategies have been used for heavy metal poisoning diagnosis,^[41] cancer diagnosis, and treatment.^[42] As a large hydrophobic molecule, PpIX is metabolized by the liver rather than excreted renally. Large amounts of PpIX are toxic to the liver and can cause cholestatic liver injury. Application of PpIX in medical diagnosis and treatment is based on its photodynamic effects. Thus, research into the PpIX molecule and its interaction with metal ions is attractive. A detailed description is available in supplementary materials S9, Supporting Information. As shown in **Figure 4**, we distinguished the combination of three metal ion species and PpIX, which can promote cellular respiration, improve protein and sugar metabolism, and resist complement binding. **Figure 4b** illustrates an increase in energy of 1.96 times at the sharp corner. Since PpIX complexes with iron, copper, or zinc ions are important for life, we investigated whether these complexes could be discriminated from one another using our sensing technique by individually injecting PpIX-Fe²⁺/Cu²⁺/Zn²⁺ solution into the

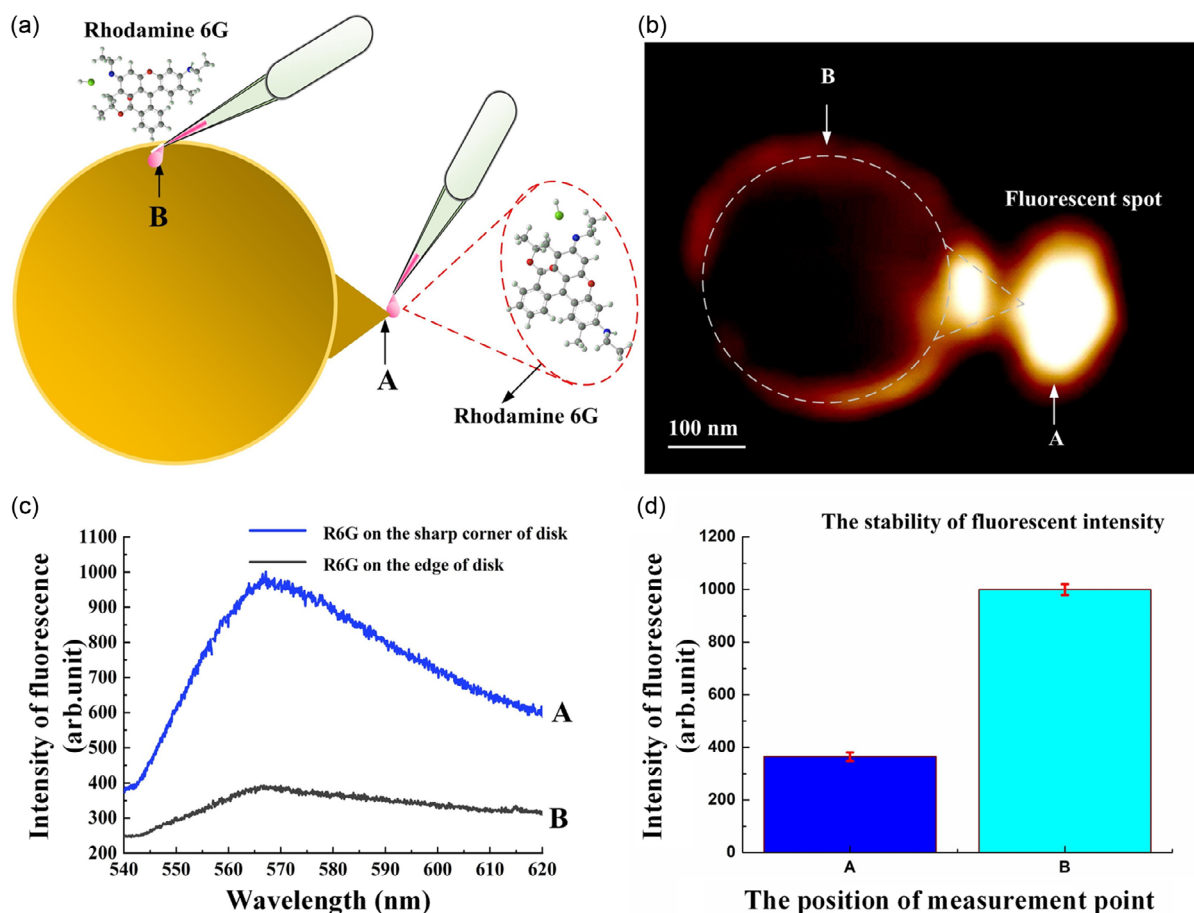


Figure 3. Applications of the nanostructures with light convergence ability. a) The illustration of detection on R6G at sharp corner and edge of disk. b) SNOM image of the manufactured nanodisk with R6G at its sharp corner (A) and edge (B). c) The corresponding spectral signals of (b). d) The stability of R6G fluorescent intensity at points A & B.

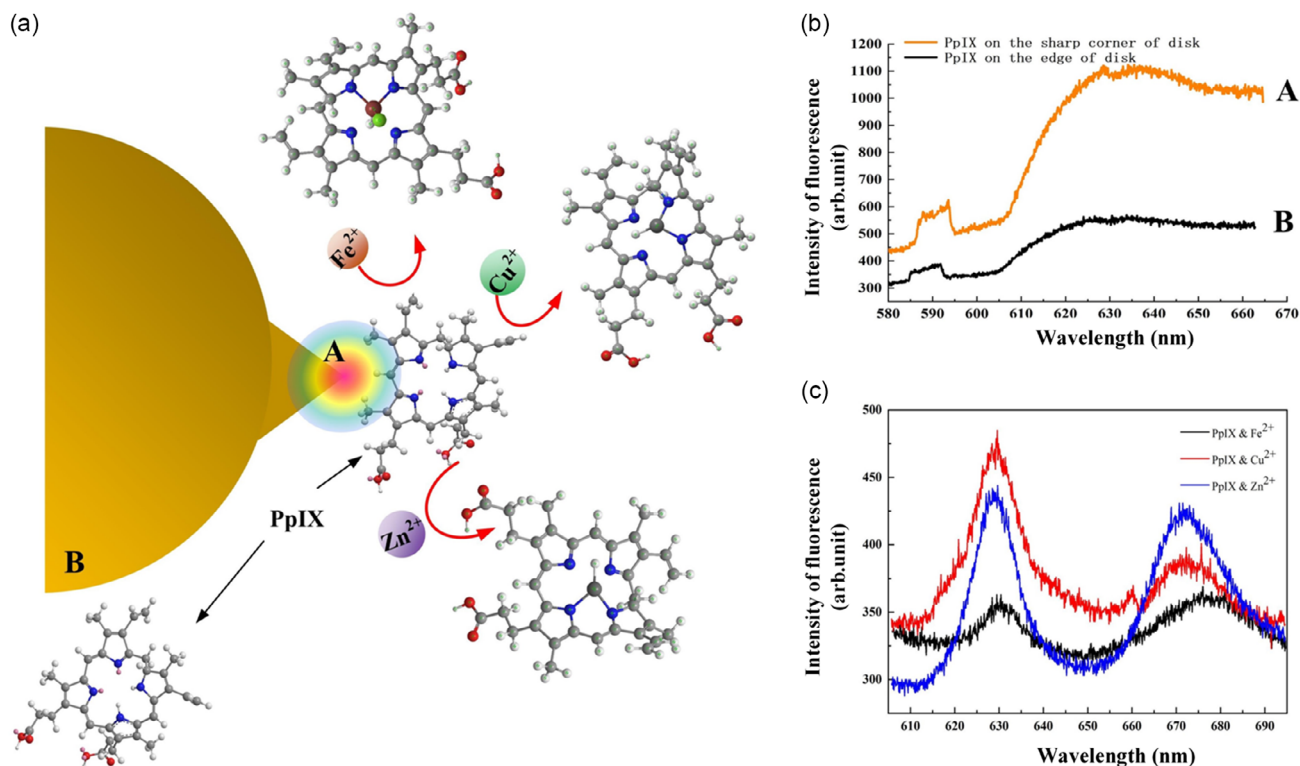


Figure 4. a) The illustration of sensing about PpIX at sharp corner (A) and edge of disk (B). b) The corresponding spectral signals of (a). c) Detection and discrimination of PpIX combined with Fe^{2+} , Cu^{2+} , and Zn^{2+} .

nanostructure. The concentration of PpIX solution was chosen to be $3.9 \times 10^{17} \text{ g mL}^{-1}$ based on observation of single-step photobleaching with R6G solution. The corresponding spectral information is presented in Figure 4c, demonstrating that the nanostructure possesses the ability to detect and distinguish different biomolecules by enhancement of fluorescence.

3. Conclusion

In conclusion, we have demonstrated the ability to transmit SPW in a simple manner. Furthermore, we have improved SPW transmission by incorporating various channels formed by long cuboid nanostructures on the surface of nanoparticles, enabling greater control over local electromagnetic fields. We have also applied cuboid nanostructures to nanodisks and observed successful excitation and transmission of SPW on their surfaces. In addition, we have designed easily fabricable nanostructures, with simulation and experimental results, demonstrating a significant enhancement of the local light field. These structures have shown potential as sensors for both nonliving components such as R6G and living components like PpIX. This research has implications for the design and development of intelligent flexible photonic materials and devices, including micro-/nanofabrication, subwavelength optics, optical data storage, and lithography. The ability to generate, transport, and control local electromagnetic fields is a critical area of research that is likely to yield further exciting developments.

4. Experimental Section

Material Preparation: The concentration of R6G solution was $4.3 \times 10^{-17} \text{ g mL}^{-1}$ in our experiment, which approached single-molecule concentrations in the 10 mL dose used. A detailed protocol for preparation of this solution is available in S10, Supporting Information. It demonstrates that the single molecule can be detected utilizing our structure by enhancement of light-matter interaction.

Device Fabrication and Measurement: Nanostructures were fabricated on substrates of SiO_2 prism by Crossbeam 540 FIB-scanning electron microscopy (SEM)-Microscopes from ZEISS and Pecs II system from GATAN. The size of SiO_2 prism was $10 \text{ mm} \times 5 \text{ mm} \times 10 \text{ mm}$, the lower surface of the prism was used for etching. Prior to etching, the surface was cleaned with 99% alcohol and sonicated with ultrasonic washing equipment to remove any attached particles. A 100 nm-thick Au seed layer was deposited on the substrate by the Pecs II system. This conductive Au layer acted as a cathode in the subsequent electroplating steps. Actually, the choice of metal and the thickness of this conductive layer were noncritical. However, Au was selected as it is resistant to oxidation and capable of maintaining strong adhesion to the SiO_2 substrate during nano-mechanical testing. The resist was then exposed using a Crossbeam 540 FIB-SEM-Microscopes system from ZEISS operating at an acceleration voltage of 10 kV. For all exposures, the beam current was maintained between 50 and 100 nA and the beam step size was 1 nm by voltage. Immediately following exposure, the surface metal was removed by wet etching method. All FIB images were generated with a 30 kV argon-ion beam with a current of $\approx 50 \text{ nA}$.

Device Fabrication and Measurement: The nanostructures were characterized by SEM, FIB imaging, and transmission electron microscopy and small-area electron diffraction (TEM and SAED, FEI Tecnai F20). SEM provided immediate confirmation of nanostructure geometry to validate the lithographic parameters, while FIB imaging was used as a primarily qualitative judgment of nanostructure. The propagation of a TM-polarized

Gaussian beam of broadband 350–950 nm multiline laser for visible and UV-A (Comblas-VIS, GLOphotonics) through the amplitude ZP with relief from chromium was experimentally studied using SNOM Ntegra Spectra (NT-MDT). The probe-coupled portion of light was then focused with a 100× objective and transmitted through spectrometer S (Solar TII, Nanofinder 30) to filter out the irrelevant radiation, before being recorded by the charge-coupled device camera (Andor. DV401-BV).

Supporting Information

Supporting Information is available from the Wiley Online Library or from the author.

Acknowledgements

The authors thank the National Natural Science Foundation of China (NSFC) (12104298 and 12192252); the Shanghai Municipal Science and Technology Major Project (grant no. 2019SHZDZX01-06); and Natural Science Foundation of Shanghai (23ZR1428400). The authors thank Jiahao Gu for the help in language polishing.

Conflict of Interest

The authors declare no conflict of interest.

Data Availability Statement

The data that support the findings of this study are available in the supplementary material of this article.

Keywords

focusing on nanotips, nanosensors, nanostructures, surface plasmon waves

Received: May 31, 2023
Revised: August 14, 2023
Published online:

- [1] L. Wang, Q. Li, *Chem. Soc. Rev.* **2018**, *47*, 1044.
[2] O. C. Farokhzad, R. Langer, *ACS Nano* **2009**, *3*, 16.
[3] S. A. Maier, *Plasmonics: Fundamentals and Applications*, Springer, New York, NY **2007**.
[4] M. G. Debije, *Adv. Funct. Mater.* **2010**, *20*, 1498.
[5] M. G. Debije, C. Menelaou, L. M. Herz, A. P. H. J. Schenning, *Adv. Opt. Mater.* **2014**, *2*, 687.
[6] C. Dahmen, B. Schmidt, G. Von Plessen, *Nano Lett.* **2007**, *7*, 318.
[7] J. Homola, *Chem. Rev.* **2010**, *108*, 426.
[8] S. Ekgasit, C. Thammacharoen, F. Yu, W. Knoll, *Anal. Chem.* **2004**, *76*, 2210.
[9] A. D. McFarland, R. P. Van Duyne, *Nano Lett.* **2003**, *3*, 1057.
[10] R. F. Aroca, D. J. Ross, C. Domingo, *Appl. Spectrosc.* **2004**, *58*, 324A.
[11] C. Noguez, *J. Phys. Chem. C* **2007**, *111*, 3806.
[12] M. A. Garcia, *J. Phys. D: Appl. Phys.* **2011**, *44*, 283001.
[13] F. J. García-Vidal, J. B. Pendry, *Phys. Rev. Lett.* **1996**, *77*, 1163.
[14] K.-Q. Lin, J. Yi, J.-H. Zhong, S. Hu, B.-J. Liu, J.-Y. Liu, C. Zong, Z.-C. Lei, X. Wang, J. Aizpurua, R. Esteban, B. Ren, *Nat. Commun.* **2017**, *8*, 14891.
[15] M. Abe, T. Suwa, *Phys. Rev. B* **2004**, *70*, 3600.
[16] Z. Jian, Z. Junwu, W. Yongchang, *Physica B* **2004**, *353*, 331.
[17] J. Hu, Y. Yu, B. Jiao, S. Ning, H. Dong, X. Hou, Z. Zhang, Z. Wu, *Org. Electron.* **2016**, *31*, 234.
[18] X. Huang, P. K. Jain, I. H. El-Sayed, M. A. El-Sayed, *Nanomedicine* **2007**, *2*, 681.
[19] L. Tong, Q. Wei, A. Wei, J. X. Cheng, *Photochem. Photobiol.* **2010**, *85*, 21.
[20] B. P. Nelson, T. E. Grimsrud, M. R. Liles, R. M. Goodman, R. M. Corn, *Anal. Chem.* **2001**, *73*, 1.
[21] K. Toshihiro, A. Ona, *Anal. Bioanal. Chem.* **2008**, *391*, 1889.
[22] L. L. Robbio, P. Uboldi, S. Marcovina, R. P. Revoltella, A. L. Catapano, *Biosens. Bioelectron.* **2001**, *16*, 963.
[23] P. Spinelli, V. E. Ferry, J. V. D. Groep, M. V. Lare, A. Polman, *J. Opt.* **2012**, *14*, 024002.
[24] M. A. Noginov, G. Zhu, A. M. Belgrave, R. Bakker, V. M. Shalaev, E. E. Narimanov, S. Stout, E. Herz, T. Suteewong, U. Wiesner, *Nature* **2009**, *460*, 1110.
[25] R. F. Oulton, V. J. Sorger, T. Zentgraf, R.-M. Ma, C. Gladden, L. Dai, G. Bartal, X. Zhang, *Nature* **2009**, *461*, 629.
[26] S. Wang, P. C. Wu, V.-C. Su, Y.-C. Lai, C. H. Chu, J.-W. Chen, S.-H. Lu, J. Chen, B. Xu, C.-H. Kuan, T. Li, S. Zhu, D. P. Tsai, *Nat. Commun.* **2017**, *8*, 187.
[27] E. Ozbay, *Science* **2006**, *311*, 189.
[28] J. A. Dionne, L. A. Sweatlock, H. A. Atwater, A. Polman, *Phys. Rev. B* **2006**, *73*, 035407.
[29] D. K. Gramotnev, M. G. Nielsen, S. J. Tan, M. L. Kurth, S. I. Bozhevolnyi, *Nano Lett.* **2012**, *12*, 359.
[30] M. Mansuripur, A. R. Zakharian, A. Lesuffleur, S. H. Oh, J. V. Moloney, *Opt. Express* **2009**, *17*, 14001.
[31] W. A. Challener, C. Peng, A. V. Itagi, D. Karns, W. Peng, Y. Peng, X. M. Yang, X. Zhu, N. J. Gokemeijer, Y.-T. Hsia, G. Ju, R. E. Rottmayer, M. A. Seigler, E. C. Gage, *Nat. Photonics* **2009**, *24*, 190.
[32] J. A. Schuller, E. S. Barnard, W. Cai, Y. C. Jun, J. S. White, M. L. Brongersma, *Nat. Mater.* **2010**, *9*, 193.
[33] X. Hao, C. Kuang, Z. Gu, Y. Wang, S. Li, Y. Ku, Y. Li, J. Ge, X. Liu, *Light Sci. Appl.* **2013**, *2*, e108.
[34] L. Li, W. Guo, Y. Yan, S. Lee, T. Wang, *Light Sci. Appl.* **2013**, *2*, 72.
[35] L. Wang, S. M. Uppuluri, E. X. Jin, X. Xu, *Nano Lett.* **2006**, *6*, 361.
[36] L. Pan, Y. Park, Y. Xiong, E. Ulin-Avila, Y. Wang, L. Zeng, S. Xiong, J. Rho, C. Sun, D. B. Bogy, X. Zhang, *Sci. Rep.* **2011**, *1*, 175.
[37] S. Molesky, Z. Lin, A. Y. Piggott, W. Jin, J. Vucković, A. W. Rodriguez, *Nat. Photonics* **2018**, *12*, 659.
[38] P. Dombi, Z. Pápa, J. Vogelsang, S. V. Yalunin, M. Sivilis, G. Herink, S. Schäfer, P. Groß, C. Ropers, C. Lienau, *Rev. Mod. Phys.* **2020**, *92*, 025003.
[39] H.-W. Liu, M. A. Becker, K. Matsuzaki, R. Kumar, S. Götzinger, V. Sandoghdar, *ACS Nano* **2022**, *16*, 12831.
[40] A. H. Atabaki, S. Moazeni, F. Pavanello, H. Gevorgyan, J. Notaros, L. Alloatti, M. T. Wade, C. Sun, S. A. Kruger, H. Meng, K. Al Qubaisi, I. Wang, B. Zhang, A. Khilo, C. V. Baiocco, M. A. Popović, V. M. Stojanović, R. J. Ram, *Nature* **2018**, *556*, 349.
[41] M. Sachar, E. Karl, *J. Pharmacol. Exp. Ther.* **2016**, *356*, 267.
[42] A. Schauder, A. Avital, Z. Malik, *J. Environ. Pathol. Toxicol. Oncol.* **2010**, *29*, 137.